Journal of Photochemistry and Photobiology A: Chemistry 227 (2012) 59–64

Contents lists available at SciVerse ScienceDirect

Journal of Photochemistry and Photobiology A: Chemistry

journal homepage: www.elsevier.com/locate/jphotochem

Noncrystalline blue-emitting 9,10-diphenylanthracene end-capped with triphenylamine-substituted fluorene

Yujian Zhang[a], Yanxian Jin[b], Ru Bai[c], Zhenwei Yu[a], Bin Hu[a], Mi Ouyang[a,*], Jingwei Sun[a], Chunhui Yu[a], Junlei Liu[a], Cheng Zhang[a,*]

[a] State Key Laboratory Breeding Base of Green Chemistry-Synthesis Technology, College of Chemical Engineering and Materials Science, Zhejiang University of Technology, Chaowang Road 18#, Hangzhou, PR China
[b] School of Pharmaceutical and Chemical Engineering, Taizhou University, Linhai, PR China
[c] School of Electronic Information, Hangzhou Dianzi University, Hangzhou, PR China

ARTICLE INFO

Article history:
Received 21 June 2011
Received in revised form
28 September 2011
Accepted 11 November 2011
Available online 20 November 2011

Keywords:
9,10-Diphenylanthracene
Hole-injection
Blue-emitting material
Thermal stability

ABSTRACT

Two blue-emitting oligomers, namely **FDPA1** and **FDPA2** containing 9,10-diphenylanthracene core end-capped with triphenylamine-substituted fluorene has been synthesized and characterized. The spiro-configuration end-capping groups imparts two compounds with pronounced morphological stability (T_g > 185 °C, T_d > 420 °C) and excellent hole injection ability (E_{HOMO} > −5.27 eV) with the advantageous optical characteristics of corresponding core. Scanning electron microscope (SEM) and X-ray diffraction (XRD) reveal that the two oligomers form excellent amorphous films and possess good morphological stability after annealing.

1. Introduction

Organic light-emitting devices (OLEDs) based on small molecules have attracted great attention in the past decades, due to their potential applications in flat-panel displays and solid state lighting resources [1–3]. Among the three primary-color emitters in OLEDs, blue-light emitting materials are of particular importance, which cannot only be used as a blue light source [4,5] but also as a host materials to generate colors else by downhill energy transfer to a suitable emissive dopant [6,7]. Unfortunately, the intrinsically wide band-gap of blue materials makes it difficult to inject carriers (holes or electrons) into emitters. As a result, the performance of blue OLEDs remains relatively poor in comparison with that of red and green OLEDs [8,9]. Additionally, the durability, which strongly depends on the thermal and morphological stability of materials, is another key factor for the device operation efficiency and lifetime [10]. Whereas, amorphous materials, thanks to their high glass transition temperature (T_g), are receiving special attention due to the effectively suppression of the crystallization for the film.

Excellent electrochemical stability and photoluminescence (PL) make anthracene derivatives attract the intensive attention and have been developed as an attractive building block and starting material in OLEDs [11–15]. Among them, 9,10-diphenylanthracene (DPA) is one of the most representative blue fluorescent materials for its excellently fluorescent properties both in solution and in the solid state [16–18]. However, an obvious deficiency of tendency to crystallize in thin film limit the further application of the DPA in blue OLEDs due to its crystal formation resulting in rough surface, grain boundaries or pin holes that eventually lead to device failure [19–21]. To date, various strategies have been developed to suppress the formation of crystal, such as the introduction of sterically hindered *t*-butyl groups [22,27], bulky substituents [21,24,25] and spiro-annulated structures [26]. Nevertheless, there are few reports on DPA derivatives end-capped with nonplanar molecular structures, which directly avoid their close packing and crystallization. Another intractable issue is the high ionization potential of anthracene-based compounds [23,27,28], which produces a relatively large hole-injection barrier from indium tin oxide (ITO) (−4.8 eV). To overcome the problem, hole-injection/transporting triarylamines were incorporated into the C2, C6 or C9, C10-positions of anthracene [28–32]. Unfortunately, such direct substitution of electron-donor groups decreases energy gap significantly due to extended conjugation lengths, which ultimately results in unwanted red-shift of

* Corresponding authors. Tel.: +86 571 88320027; fax: +86 571 88320027.
E-mail addresses: ouyang@zjut.edu.cn (M. Ouyang), czhang@zjut.edu.cn (C. Zhang).

1010-6030/$ – see front matter © 2011 Elsevier B.V. All rights reserved.
doi:10.1016/j.jphotochem.2011.11.003

emission peak. Thus, the development of new approaches that can lead to stabilization of amorphous state and excellent hole-injection/transportation ability is particularly critical for obtaining highly efficient blue-emitting anthracene-based materials without the decrease of optical performance.

In this contribution, the synthesis and physical and chemical properties of two thermally stable materials **FDPA1**and **FDPA2** (Scheme 1), containing DPA as main core unit, are reported. End-capping triphenylamine (TPA)-substituted fluorene (TPAF) is incorporated into DPA unit to retain the large band gap of the original DPA core. In addition, end-capping fluorene and TPA moieties are connected through the sp^3-hybridized carbon atom, which may not only hinder close packing and crystallization but also result in pronounced morphological stability of amorphous materials. Meanwhile, the hole-injection/transportation ability of molecules is efficiently improved.

2. Experimental

2.1. Chemicals and instruments

9-(4-Bromophenyl)-fluoren-9-ol [33] and 2,6-dibromoanthracene-9,10-dione [28] were synthesized as reported previously. All chemical reagents were used as received from commercial sources without further purification. And the solvents used in the reaction were purified following routine procedures. ^{1}H and ^{13}C NMR spectra were recorded on Bruker Avance III 500-MHz spectrometer using the chloroform-d as the solvent. High-resolution mass spectrometric measurements were carried out on a Brüker autoflex MALDI-TOF-MS spectrometer. Elemental analyses were performed using the Thermo-Finnigan Flash EA-1112 (CE, Italy) instrument. UV–vis spectra were measured using a Shimadzu UV-1800 spectrophotometer. PL spectra were obtained using a Perkin-Elmer LS-55 luminescence spectrophotometer. Thermal analysis was performed on a Diamond TG/DTA 6300 (PerkinElmer, USA) in the temperature range of 100–800 °C. The differential scanning calorimetry (DSC) analysis was performed on a TA Instruments DSC2920. A CHI 660C electrochemical analyzer was applied to conduct the electrochemical measurements. X-ray diffraction (XRD) measurements of thin films were performed on X'Pert Pro diffractometer.

2.2. Synthesis

2.2.1. 2,6-Dibromo-9,10-bis(4-butylphenyl)anthracene (*BrDPA*) [31]

The 1-bromo-4-butylbenzene (2.12 g, 10 mmol) dissolved in diethyl ether (100 mL) was mixed with 6.25 mL of n-butyllithium (1.6 M in hexane) in diethyl ether (100 mL) at −78 °C. To the suspension, 2,6-dibromoanthraquinone (1.8 g, 5.0 mmol) in diethyl ether (20 mL) was added dropwise at −78 °C. After stirring for 1 h at the room temperature, the mixture was poured into an aqueous HCl solution (2 M) and the organic phase separated. The water phase was extracted with ether (3 × 50 mL). The combined organic fractions were dried over magnesium sulfate and the diethyl ether was removed to get residue. And then, to this residue were added potassium iodide (3.0 g, 18 mmol), $Na_2H_2PO_2$ (3.0 g, 34 mmol), and acetic acid (30 mL), and the mixture was heated under reflux for 3 h. The precipitated product in the reaction vessel was filtered with a glass filter and washed with water to give compound BrDPA (0.92 g, 30.7%).

^{1}H NMR (500 MHz, $CDCl_3$) δ 7.86 (d, J = 2.0 Hz, 2H), 7.58 (d, J = 9.5 Hz, 2H), 7.43 (d, J = 8.0 Hz, 4H), 7.38 (dd, J = 10.5 Hz, 2H), 7.33 (d, J = 8.0 Hz, 4H), 2.85–2.78 (m, 4H), 1.80 (dt, J = 15.5, 4H), 1.52 (dd, J = 14.5 Hz, 4H), 1.05 (t, J = 7.5 Hz, 6H); ^{13}C NMR (500 MHz, $CDCl_3$) δ 142.7, 136.9, 134.8, 131.1, 131.0, 129.1, 129.0, 128.8, 128.7, 120.7, 35.6, 33.6, 22.6, 14.1. **MS(EI)**: m/e 600.1(M^+).

2.2.2. 4-(9-(4-Bromophenyl)-fluoren-9-yl)-N,N-di-p-tolylaniline (*4*)

A solution of CF_3SO_3H (1.84 mL, 20 mmol) in appropriate 1,4-dioxane (20 mL) was added drop wise to a mixture solution of **3** (3.4 g, 10 mL) [33] and N,N-Bis(4-methylphenyl)aniline (2.7 g, 10 mmol) in 1,4-dioxane (80 mL). The reaction mixture was stirred at 80 °C under nitrogen until starting material was no longer detectable by TLC (8 h). The mixture was poured into saturated $NaHCO_3$ solution and extracted with $CHCl_3$. After the crude product was further purified by column chromatography (EtOAc/hexane = 1/20) to give the desired product **4** (4.6 g, 77.8%).

^{1}H NMR (500 MHz, $CDCl_3$) δ 7.78 (d, J = 7.5 Hz, 2H), 7.42–7.33 (m, 6H), 7.32–7.26 (m, 2H), 7.11 (d, J = 8.5 Hz, 2H), 7.05 (d, J = 8.5 Hz, 4H), 6.99 (dd, J = 10.5 Hz, 6H), 6.87 (d, J = 8.5 Hz, 2H), 2.31 (s, 6H); ^{13}C NMR ($CDCl_3$ 500 MHz) δ 151.0, 146.9, 145.4, 145.1, 140.0, 137.6, 132.5, 131.2, 129.9, 129.8, 128.6, 127.7, 127.6, 126.0, 124.7, 121.8, 120.6, 120.2, 64.5, 20.8; **MS(EI)**: m/e 591.2(M^+).

2.2.3. 4-Methyl-N-(4-(9-(4-(4,4,5,5-tetramethyl-1,3,2-dioxaborolan-2-yl)phenyl)-fluoren-9-yl)phenyl)-N-(p-tolyl)aniline (*5*)

4 (3 g, 5 mmol), 4,4,4′,4′,5,5,5′,5′-octamethyl-2,2′-bis(1,3,2-dioxaborolane) (1.3 g, 5.2 mmol), KOAc (1.4 g, 14.2 mmol), and $Pd(dppf)Cl_2$ (30 mg) were mixed in anhydrous DMSO (25 mL). Then, the mixture was degased by purging with N_2. The solution was heated at 80 °C for 24 h under N_2. After the reaction mixture cooled, the solvent was evaporated and the product was extracted with chloroform. The organic extracts were washed with brine, and then dried over $MgSO_4$. After, the solvent was evaporated. Finally, the crude product was purified through columnchromatography (hexane/EtOAc, 12:1) to give **5** (1.4 g, 45%).

^{1}H NMR (500 MHz, $CDCl_3$) δ 7.77 (d, J = 7.5 Hz, 2H), 7.69 (d, J = 8.0 Hz, 2H), 7.41 (d, J = 7.5 Hz, 2H), 7.39–7.23 (m, 6H), 7.04 (d, J = 8.5 Hz, 4H), 6.99 (dd, J = 15 Hz, 6H), 6.85 (d, J = 8.5 Hz, 2H), 2.30 (s, 6H), 1.32 (s, 12H); ^{13}C NMR ($CDCl_3$ 500 MHz) δ 151.2, 149.5, 146.7, 145.2, 140.1, 138.3, 134.7, 132.4, 129.8, 128.7, 127.5, 127.4, 126.2, 124.6, 121.9,120.1, 83.7, 65.2, 24.8, 20.8; **MS(EI)**: m/e 639.2(M^+).

2.2.4. General procedure for the synthesis of compounds *FDPA1, FDPA2*

A mixture of anthracene-based core (1 mmol), **5** (1.4 g, 2.2 mmol), $Pd(PPh_3)_4$ (0.3 g, 0.27 mmol), Na_2CO_3 (2.0 M, 3.0 mL), and toluene (50 mL)/THF (30 mL) was stirred at 90 °C for 48 h under the atmosphere of nitrogen. After the mixture cooled, 200 mL of $CHCl_3$ was added to the reaction mixture. The organic portion was separated and washed with brine before dried over anhydrous $MgSO_4$. The solvent was evaporated off, and the solid residues were purified by column chromatography to afford the desired product.

FDPA1 (0.73, 60.8%); ^{1}H NMR (500 MHz, $CDCl_3$) δ 7.84 (d, J = 7.5 Hz, 4H), 7.66 (dd, J = 6.5 Hz, 4H), 7.61 (d, J = 7.5 Hz, 4H), 7.44 (m, 8H), 7.38 (t, J = 7.5 Hz, 4H), 7.30 (dd, J = 14.5 Hz, 8H), 7.14 (d, J = 8.5 Hz, 4H), 7.05 (d, J = 8.5 Hz, 8H), 7.00 (d, J = 8.5 Hz, 8H), 6.93 (d, J = 8.5 Hz, 4H), 2.30 (s, 12H); **MALDI-TOF-MS** (m/z) 1200.5(M^+); **Anal. Calcd** for $C_{92}H_{68}N_2$: C, 91.96; H, 5.70; N, 2.33 Found: C, 91.89; H, 5.88; N, 2.23.

FDPA2 (0.46, 31.7%); ^{1}H NMR (500 MHz, $CDCl_3$) δ 7.88 (s, 2H), 7.76 (t, J = 8.5 Hz, 6H), 7.57 (dd, J = 9.0, 2H), 7.43 (t, J = 7.5 Hz, 8H), 7.41–7.34 (m, 12H), 7.29 (d, J = 7.5 Hz, 2H), 7.23–7.8 (m, 6H), 7.04 (d, J = 8.0 Hz, 12H), 6.97 (d, J = 7.5 Hz, 8H), 6.86 (d, J = 8.0 Hz, 4H),

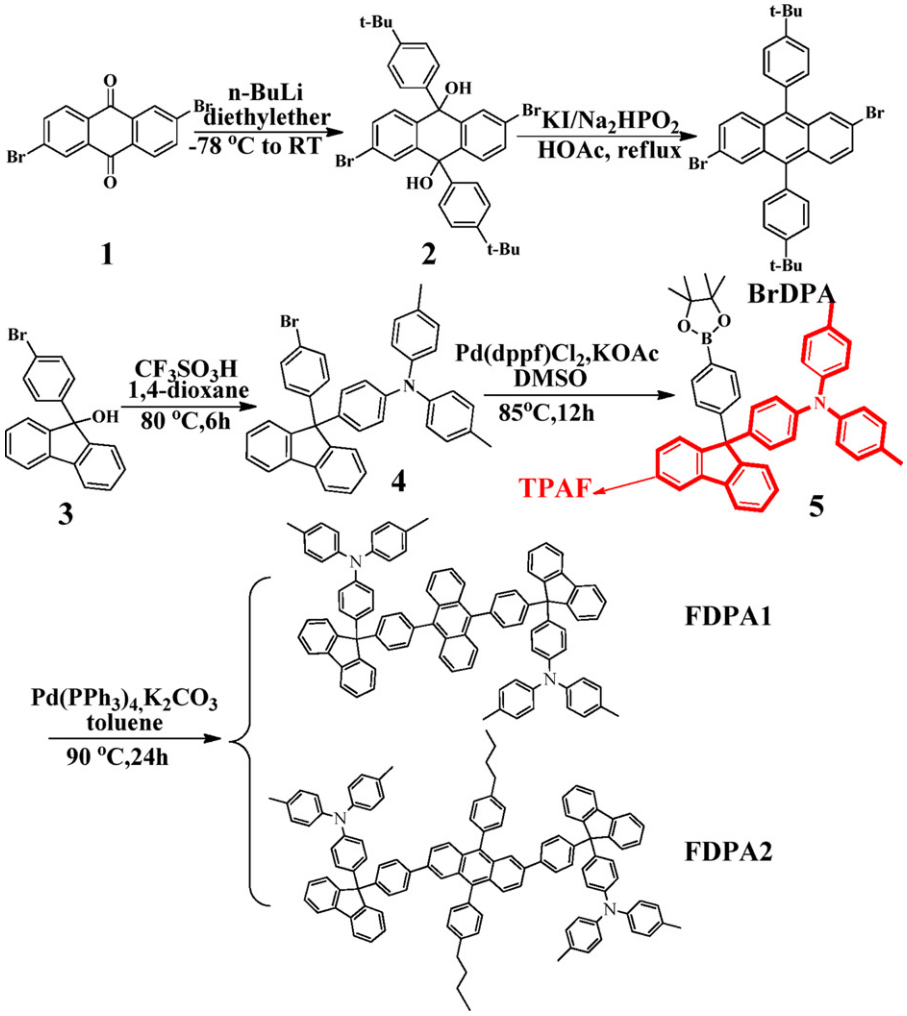

Scheme 1. Syntheses of compounds **FDPA1** and **FTPA2**.

2.80 (t, J = 7.5 Hz, 4H), 2.30 (s, 12H), 1.75–1.79 (m, 4H), 1.45–1.51 (m, 4H), 1.02 (t, J = 7.5 Hz, 6H); **MALDI-TOF-MS** (m/z) 1465.7 (M^+); **Anal. Calcd** for $C_{111}H_{92}N_2$: C, 91.76; H, 6.33; N, 1.91 Found: C, 91.89; H, 6.14; N, 1.97.

3. Results and discussion

3.1. Synthesis and characterization

Scheme 1 illustrates the synthetic route for the preparation of DPA derivative consisting of a DPA core and two TPA-substituted fluorene peripheries. The Grignard reaction of fluorenone with (*p*-bromophenyl)-magnesium bromide gave the corresponding tertiary alcohol **3**. Acid-promoted Friedel–Crafts type substitution of N,N-Bis(4-methylphenyl)aniline with **3** afforded bromide **4** in high yield. Subsequently, the compound **4** underwent cross-coupling reaction with the pinacol ester of diboron to give the key intermediate arylboronic ester. Ultimately, the Pd-catalyzed Suzuki coupling reaction was employed between arylboronic ester and 9,10-dibromo-anthracene or dibromide **BrTPA** to afford the corresponding compounds **FDPA1** or **FDPA2** with 60.8% and 31.7% yield, respectively. Elemental analysis, ^{1}H NMR and MALDI-TOF-MS were utilized to confirm the structure. Unfortunately, the target compounds did not show excellent solubility, thus, no ^{12}C NMR spectra were available in common organic solvent.

3.2. Photophysical properties

Fig. 1 presented the UV–vis absorption and PL spectra of **FDPA1** and **FDPA2** recorded both in chloroform solution and the film state. The absorption bands ranging from 288 to 350 nm could be attributed to the n–π* transition of the peripheral end-capping groups [34]. Additionally, their characteristic vibronic bands in the region from 350 to 450 nm were assigned to the π–π* transitions of the anthracene core [23]. Herein, it was noteworthy that the π–π* absorption transitions were slightly red-shifted by 2 nm for **FDPA1** and 1 nm for **FDPA2** compared to that of DPA [35] as well as Ph-DPAN [28], respectively. Interestingly, in comparison with Ph-DPAN, the emission peaks at 446.6 nm for **FDPA2** showed an evident blue-shift due to the weak intermolecular interactions. The results clearly confirmed that the introduction of end-capping groups did not lead to the expansion of conjugation remarkably. In contrast, the PL emission wavelength of two oligomers presented slight red-shift from solution to solid film. Besides, the full widths at half maximum (FWHM) were 56.6 and 55.8 nm for **FDPA1**, 58.9 and 69.4 nm for **FDPA2** in solution and in the film respectively. The similarity in the FWHM and the small difference between the emission peak of sample in the solution and solid state implied that the bulky end-capping TPAF groups effectively enhanced steric hindrance, which significantly hindered the chose packing and molecular interactions resulting in fluorescence quenching. Moreover, the peripheral end-capping groups with a negligible conjugation with

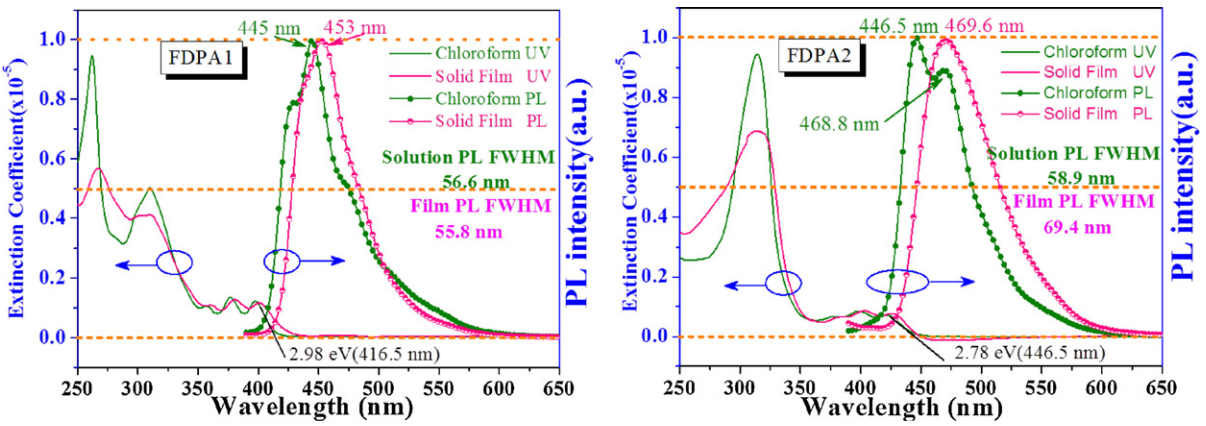

Fig. 1. The absorption and PL spectra of the target compounds in solution and in film.

the DPA core effectively retained the large band gap of the original DPA. The fluorescence quantum yields (Φ_F) of **FDPA1** and **FDPA2** were measured as 0.67 and 0.62, respectively, in dilute chloroform solutions using DPA (Φ_F = 0.9, in cyclohexane) as a standard. The optical energy band-gaps **FDPA1** and **FDPA2** were 2.98 and 2.78 eV, respectively.

3.3. Electrochemical properties

As shown in Fig. 2, cyclic voltammetry (CV) was performed to examine the electrochemical properties of the obtained oligomers. The anode scans demonstrated similar values of onset oxidation potential (E_{OX}) for both DPA-based oligomer (0.90 V for **FDPA1** and 0.89 V for **FDPA2**). To assess the charge injecting properties, the estimated HOMO energy levers were −5.28 eV for **FDPA1** and −5.27 eV for **FDPA2**, respectively (HOMO = −(E_{OX} + 4.38 eV)). The LUMO energy levers of **FDPA1** and **FDPA2** were −2.30 and −2.49 eV, respectively, calculated from HOMO energy level and energy gap (E_g) determined from the threshold of the optical absorption. The results demonstrated that the high HOMO energy level of FDPA1-2 greatly reduced the energy barrier for hole-injection from the ITO anode (W_{ITO} = −4.8 eV) to and the emissive chromophore. Additionally, the conjugation length and structure of the core had little influence on the ability of hole-injection of materials. Fig. 2 also showed the reversible p-doping processes of compounds, indicating the high stability for hole-injection of the emissive materials. Under successive multiple potential scans (10 scans), the CV curves remained less change, demonstrated the excellent electrochemical stability of the as-prepared materials. In short, the incorporation of TPA-based end-caps effectively improved the hole transport/injection ability of DPA without obvious altering energy gap of the corresponding core, DPA and Ph-DPAN.

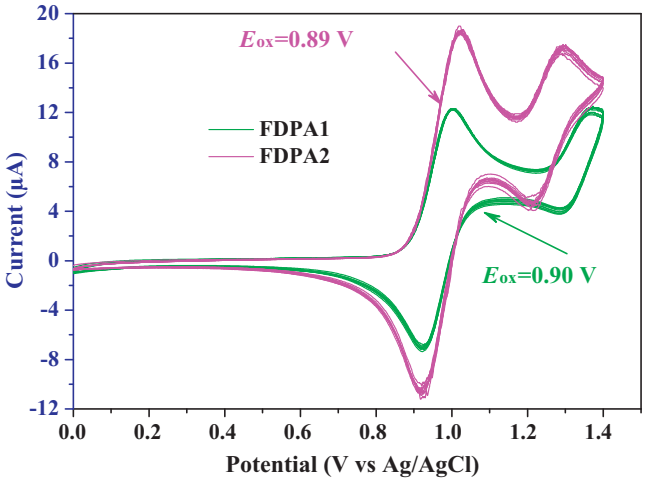

Fig. 2. Cyclic voltammograms of compounds **FDPA1** and **FDPA2** (10 scans) in CH_2Cl_2 with 0.10 M of TBAP as a supporting electrolyte, scan rate 50 mV s^{-1}.

3.4. Theoretical estimation of molecular orbitals

The optimized geometries and spatial distributions of **FDPA1** and **FDPA2** were calculated by means of density functional theory (DFT) at the level of B3LYP/6-31G(d). The bulky phenyl and triarylamines group at the 9-position of fluorene were significantly twisted toward the fluorene backbone, resulting in a noncoplanar structure, as shown in Fig. 3. This three-dimensionally non-coplanar conformation hindered intermolecular interactions effectually and thus, suppressed molecular crystallize and improve morphological stability of thin film. Moreover, the fluorene and phenyl moieties were connected through the sp3-hybridized carbon atom at the 9-position of fluorene, which effectively blocked the conjugation between them. These theoretical results were consistent with the above experimental results. The HOMO orbitals were predominantly concentrated on the triphenylamino group. For compound **FDPA1**, the LUMO orbitals were mainly located on the DPA core. However, for oligomer **FDPA2**, the electron density distributions of the LUMO were partially spread to phenyl moieties at the 3- and 6-positions of the anthracene. The above-mentioned results strongly explained the phenomena that the HOMO level of **FDPA1** was higher than that of **FDPA2**. Consequently, the molecular orbital analysis clearly proved our molecular design strategy was effective.

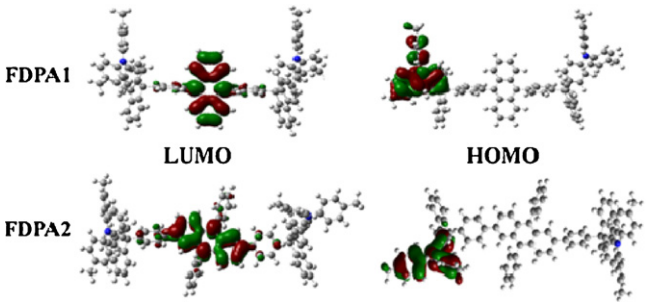

Fig. 3. Pictorial representations of Frontier molecular orbitals calculated at B3LYP/6-31G for compounds **FDPA1** and **FDPA2**.

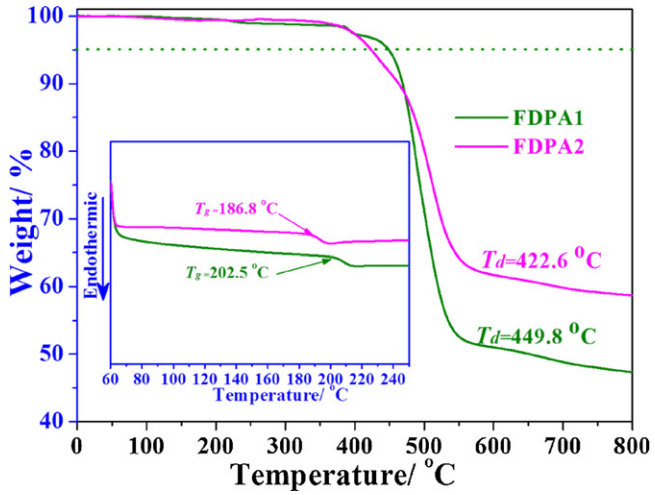

Fig. 4. TGA and DSC thermogram of the oligomers under a nitrogen atmosphere with heating rate of 10 °C min^{-1}.

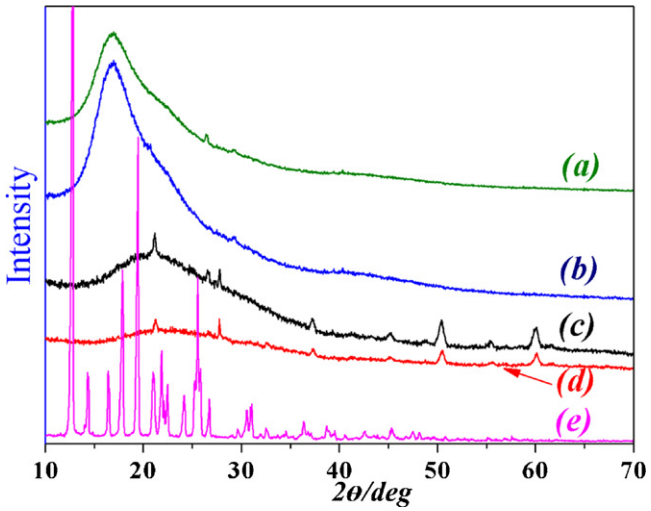

Fig. 6. X-ray diffraction patterns of the samples: (a) **FDPA1** film and (b) after heating to 100 °C for 10 h; (c) **FDPA2** film and (d) after heating to 100 °C for 10 h; (e) film for DPA.

3.5. Thermal properties

The thermal properties of the nonplanar oligomers were investigated by thermogravimetric analysis (TGA) and differential scanning calorimetry (DSC), as shown in Fig. 4. Two oligomers, **FDPA1** and **FDPA2** possessed thermal decomposition temperature (T_d: 5% weight loss) as high as 422.6 and 449.8 °C respectively, which were higher than that of the corresponding core, **DPA** and **Ph-DPAN** [28,35]. With the second heating scan, the glass transition at 186.8 °C for **FDPA1** and 202.5 °C for **FDPA2**, was observed evidently. These observations indicated that the enhanced thermal stability of amorphous films was attributed to the existence of the rigid fluorene end-caps, which effectually suppressed the tendency to crystallization and increased the T_g of compounds. In general, the higher for T_g and T_d of light-emitting materials, the film morphological properties are the more stable during the operation of the device.

To further confirm the rationality of our molecular design strategy, the thin films were prepared on the surface of ITO via spin-coating. The morphological stability of **FDPA1** and **FDPA2** was systematically investigated by scanning electron microscope (SEM) and X-ray diffraction (XRD). The surface morphologies in Fig. 5a and b clearly revealed that the films exhibited fairly smooth and uniform surface. In contrast, DPA film in Fig. 5c displayed a rough surface dotted with lots of crystal block. These images provided the intuitive evidence that the presence of the peripheral end-capping groups effectively reduced the tendency to crystallization. Expectably, the XRD results were in agreement with the proposals above. As shown in Fig. 6e, the XRD curve of the DPA film exhibited sharp and intense reflections, indicating excellent crystallinity of the film. However, a weak, broad, and diffused peak was observed in the thin film of **FDPA1** and **FDPA2** (Fig. 6a and c), presented the degradation crystallinity of the film or might be even amorphous. More importantly, there was negligible morphological change on

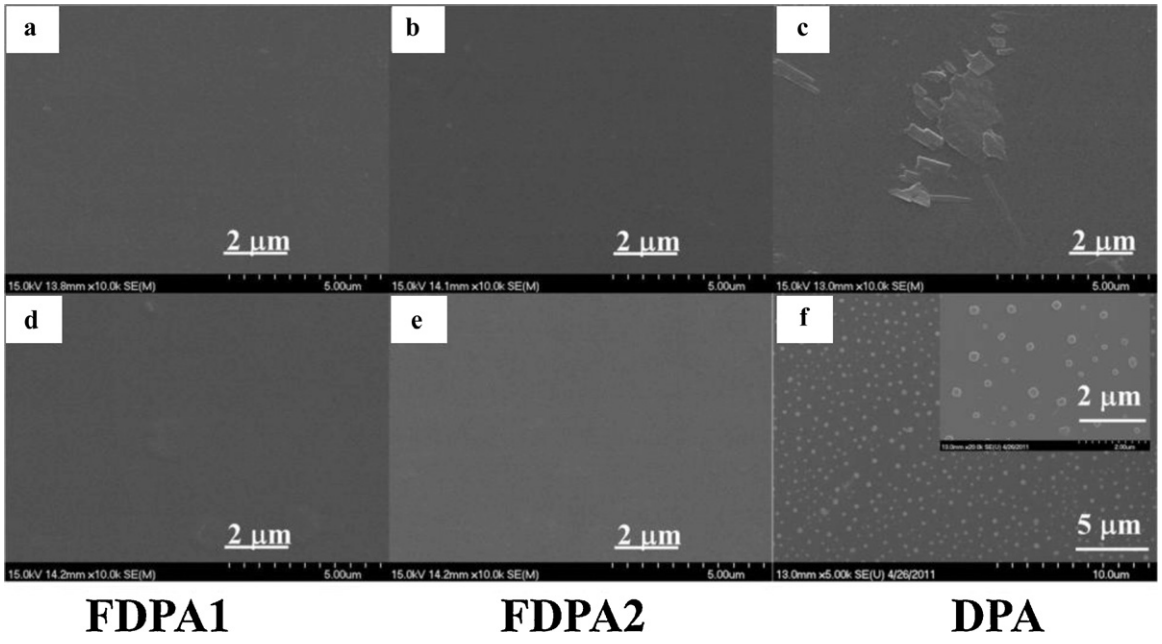

Fig. 5. SEM images of **FDPA1**, **FDPA2** and DPA films; top, before heated (a–c); down, after heated at 100 °C (d–f) for 10 h under air atmosphere. Inset in (f) is the magnified SEM images.

the **FDPA1** and **FDPA2** film after annealed at 100 °C for 10 h under air atmosphere as shown in Fig. 5d and e, respectively. The XRD pattern of the heated sample was nearly the same as that of the original sample except for the slight changes in diffraction peaks intensity (Fig. 6b and d). As a comparison, DPA film suffered obvious crystallizing after the same thermal treating, and large-scale quadrate particles with edge length ranging from 0.5 to 1.2 μm were observed in Fig. 5f. The above results further indicated the thermal stability of oligomers **FDPA1** and **FDPA2** was better than that of corresponding core. The presence of the end-capping **TPAF** group hindered close packing and crystallization may be the reason for the increase of film morphological stability.

4. Conclusions

In conclusion, two novel non-coplanar oligomers containing DPA unit as the core and two TPAF units as the peripheries were facilely prepared by Suzuki coupling and Friedel–Crafts reaction. Amorphous and spiro-configuration molecular gives excellent performances, such as good thermal, morphological stabilities, excellent fluorescence quantum yield and wide energy gap, to the two blue-emitting oligomers. Additionally, the presence of TPA improved the hole-injection and -transporting ability of the resulting materials. Therefore, it is reasonably inferred that a novel class of blue-emitting materials with excellent thermal and electrochemical stability, high fluorescence quantum yield as well as high HOMO energy levels is expected to be achieved via this end-capping strategy.

Acknowledgements

The authors gratefully thank the support of National Basic Research Program of China (2010CB635108, 2011CBA00700), Natural Science Foundation of Zhejiang Province, China (Y4090260), Major Science and Technology, Special and Priority Themes of Zhejiang Province, China (2009C14004).

References

[1] C.W. Tang, S.A. Vanslyke, Organic electroluminescent diodes, Appl. Phys. Lett. 51 (1987) 913–915.
[2] F.C. Chen, T. Yang, M.E. Thompson, J. Kido, High-performance polymer light-emitting diodes doped with a red phosphorescent iridium complex, Appl. Phys. Lett. 80 (2002) 2308–2310.
[3] X.H. Zhu, J.B. Peng, Y. Cao, J. Roncali, Solution-processable single-material molecular emitters for organic light-emitting devices, Chem. Soc. Rev. 40 (2011) 3509–3524.
[4] C. Huang, C.G. Zhen, S.P. Su, K.P. Loh, Z.K. Chen, Solution-processable polyphenyl phenyl dendron bearing molecules for highly efficient blue light-emitting diodes, Org. Lett. 7 (2005) 391–394.
[5] C.J. Tonzola, A.P. Kulkarni, A.P. Gifford, W. Kaminsky, S.A. Jenekhe, Blue-light-emitting oligoquinolines: synthesis, properties, and high-efficiency blue-light-emitting diodes, Adv. Funct. Mater. 17 (2007) 863–874.
[6] Z.Q. Gao, B.X. Mi, C.H. Chen, K.W. Cheah, Y.K. Cheng, W.S. Wen, High-efficiency deep blue host for organic light-emitting devices, Appl. Phys. Lett. 90 (2007) 123506–123508.
[7] R. Meerheim, K. Walzer, M. Pfeiffer, K. Leo, Ultrastable and efficient red organic light emitting diodes with doped transport layers, Appl. Phys. Lett. 89 (2006) 061111–061113.
[8] S. Tang, M.R. Liu, P. Lu, H. Xia, M. Li, Z.Q. Xie, F.Z. Shen, C. Gu, H.P. Wang, B. Yang, Y.G. Ma, A molecular glass for deep-blue organic light-emitting diodes comprising a 9,9′-spirobifluorene core and peripheral carbazole groups, Adv. Funct. Mater. 17 (2007) 2869–2877.
[9] H.C. Li, Y.P. Lin, P.T. Chou, Y.M. Cheng, R.S. Liu, Color tuning and highly efficient blue emitters of finite diphenylamino-containing oligo(arylenevinylene) derivatives using fluoro substituents, Adv. Funct. Mater. 17 (2007) 520–530.
[10] F. Steuber, J. Staudigel, M. Stoessel, J. Simmerer, A. Winnacker, H. Spreitzer, F. Weissoertel, J. Salbeck, White light emission from organic LEDs utilizing spiro compounds with high-temperature stability, Adv. Mater. 12 (2000) 130–133.
[11] A. Marrocchia, A. Spalletti, S. Ciorbaa, M. Seri, F. Elisei, A. Taticchia, Synthesis and photo-physical properties of conjugated anthracene-based compounds, J. Photochem. Photobiol. A 211 (2010) 162–169.
[12] S.H. Lin, F.I. Wu, R.S. Liu, Synthesis, photophysical properties and color tuning of highly fluorescent 9,10-disubstituted-2,3,6,7-tetraphenylanthracene, Chem. Commun. 696 (2009) 1–6963.
[13] Z.J. Zhao, J.H. Li, P. Lu, Y. Yang, Fluorescent, carrier-trapping dopants for highly efficient single-layer polyfluorene LEDs, Adv. Funct. Mater. 17 (2007) 2203–2210.
[14] J.H. Huang, B. Xu, J. Hua Su, C.H. Chen, H. Tian, Efficient blue lighting materials based on truxene-cored anthracene derivatives for electroluminescent devices, Tetrahedron 66 (2010) 7577–7582.
[15] D. Kumar, K.R.J. Thomas, Optical properties of pyrene and anthracene containing imidazoles: experimental and theoretical investigations, J. Photochem. Photobiol. A 218 (2011) 162–173.
[16] K.M. Omer, S.Y. Ku, K.T. Wong, A.J. Bard, Efficient and stable blue electro generated chemiluminescence of fluorene-substituted aromatic hydrocarbons, Angew. Chem. Int. Ed. 48 (2009) 9300–9303.
[17] J.H. Huang, J.H. Su, X. Li, M.K. Lam, K.M. Fung, H.H. Fan, K.W. Cheah, C.H. Chen, H. Tian, Bipolar anthracene derivatives containing hole- and electron-transporting moieties for highly efficient blue electroluminescence devices, J. Mater. Chem. 21 (2011) 2957–2964.
[18] V.H. Gessner, T.D. Tilley, Diphenylanthracene macrocylces from reductive zirconocene coupling: on the edge of steric overload, Org. Lett. 5 (2011) 1154–1157.
[19] Y.Y. Lyu, J. Kwak, O. Kwon, S.H. Lee, D. Kim, C. Lee, K. Char, Silicon-cored anthracene derivatives as host materials for highly efficient blue organic light-emitting devices, Adv. Mater. 20 (2008) 2720–2729.
[20] T.H. Liu, W.J. Shen, C.K. Yen, C.Y. Iou, H.H. Chen, B. Banumathy, C.H. Chen, Doped blue emitters of 9,10-di(2-naphthyl)anthracene in organic electroluminescent devices, Synth. Met. 137 (2003) 1033–1034.
[21] Y.H. Kim, H.C. Jeong, S.H. Kim, K. Yang, S.K. Kwon, High-purity-blue and high-efficiency electroluminescent devices based on anthracene, Adv. Funct. Mater. 15 (2005) 1799–1805.
[22] M.R. Zhu, Q. Wang, Y. Gu, X.S. Cao, C. Zhong, D.G. Ma, J.G. Qin, C.L. Yang, Efficient deep-blue emitters comprised of an anthracene core and terminal bifunctional groups for nondoped electroluminescence, J. Mater. Chem. 21 (2011) 6409–6415.
[23] Z.Y. Xia, J.H. Su, W.Y. Wong, L. Wang, K.W. Cheah, H. Tian, C.H. Chen, High performance organic light-emitting diodes based on tetra(methoxy)-containing anthracene derivatives as a hole transport and electron-blocking layer, J. Mater. Chem. 20 (2010) 8382–8388.
[24] S.L. Tao, Y.C. Zhou, C.S. Lee, S.T. Lee, D. Huang, X.H. Zhang, Highly efficient non-doped blue organic light-emitting diodes based on anthracene-triphenylamine derivatives, J. Phys. Chem. C 112 (2008) 14603–14606.
[25] J.H. Huang, B. Xua, M.K. Lam, K.W. Cheah, C.H. Chen, J.H. Su, Unsymmetrically amorphous 9,10-disubstituted anthracene derivatives for high-efficiency blue organic electroluminescence devices, Dyes Pigments 89 (2011) 155–161.
[26] W.J. Shen, R. Dodda, C.C. Wu, F.I. Wu, T.H. Liu, H.H. Chen, C.H. Chen, C.F. Shu, Spirobifluorene-linked bisanthracene: an efficient blue emitter with pronounced thermal stability, Chem. Mater. 16 (2004) 930–934.
[27] M.A. Reddy, A. Thomas, K. Srinivas, V.J. Rao, K. Bhanuprakash, B. Sridhar, A. Kumar, M.N. Kamalasanan, R. Srivastava, Synthesis and characterization of 9,10-bis(2-phenyl-1,3,4-oxadiazole) derivatives of anthracene: efficient n-type emitter for organic light-emitting diodes, J. Mater. Chem. 19 (2009) 6172–6184.
[28] W.J. Jo, K.H. Kim, H.C. No, D.Y. Shin, S.J. Ohb, J.H. Sonb, Y.H. Kimc, Y.K. Cho, Q.H. Zhao, K.H. Lee, H.Y. Oh, S.K. Kwon, High efficient organic light emitting diodes using new 9,10-diphenylanthracene derivatives containing bulky substituents on 2,6-positon, Synth. Met. 159 (2009) 1359–1364.
[29] K.H. Lee, J.N. You, S. Kang, J.Y. Lee, H.J. Kwon, Y.K. Kim, S.S. Yoon, Synthesis and electroluminescent properties of blue-emitting t-butylated bis(diarylaminoaryl)anthracenes for OLEDs, Thin Solid Films 518 (2010) 6253–6258.
[30] M.X. Yu, J.P. Duan, C.H. Lin, C.H. Cheng, Y.T. Tao, Diaminoanthracene derivatives as high performance green host electro-luminescent materials, Chem. Mater. 14 (2002) 3958–3963.
[31] K. Danel, T.H. Huang, J.T. Lin, Y.T. Tao, C.H. Chuen, Blue-emitting anthracenes with end-capping diarylamines, Chem. Mater. 14 (2002) 3860–3865.
[32] K.M. Omer, S.Y. Ku, J.Z. Cheng, S.H. Chou, K.T. Wong, A.J. Bard, Electrochemistry and electrogenerated chemiluminescence of a spirobifluorene-based donor (triphenylamine) acceptor (2,1,3-benzothiadiazole) molecule and its organic nanoparticles, J. Am. Chem. Soc. 133 (2011) 5492–5499.
[33] C. Zhang, Y.J. Zhang, W.Q. Xiang, B. Hu, M. Ouyang, Y. Xu, C. Ma, The construction of H-shaped fluorescent materials based on building blocks consisting of triphenylamine and fluorene, Chem. Lett. 39 (2010) 520–521.
[34] P.I. Shih, C.H. Chien, F.I. Wu, C.F. Shu, A novel fluorene-triphenylamine hybrid that is a highly efficient host material for blue-green-, and red-light-emitting electrophosphorescent devices, Adv. Funct. Mater. 17 (2007) 3514–3520.
[35] S.H. Ye, J.M. Chen, C.A. Di, Y.Q. Liu, K. Lu, W.P. Wu, C.Y. Du, Y. Liu, Z.G. Shuai, G. Yu, Phenyl-substituted fluorene-dimer cored anthracene derivatives: highly fluorescent and stable materials for high performance organic blue- and white-light-emitting diodes, J. Mater. Chem. 20 (2010) 3186–3194.